Multiscale damage analysis of carbon nanotube nanocomposite using a continuum damage mechanics approach

Ashwin Rai, Nithya Subramanian, Bonsung Koo and Aditi Chattopadhyay

School for Engineering of Matter, Transport, and Energy, Arizona State University, USA

Corresponding author: Aditi Chattopadhyay, School for Engineering of Matter, Transport, and Energy, Arizona State University, Tempe, AZ 85287, USA. Email: aditi@asu.edu

Abstract

A multiscale-modeling framework is presented to understand damage and failure response in carbon nanotube reinforced nanocomposites. A damage model is developed using the framework of continuum damage mechanics with a physical damage evolution equation inspired by molecular dynamics simulations. This damage formulation is applied to randomly dispersed carbon nanotube reinforced nanocomposite unit cells with periodic boundary conditions to investigate preferred sites and the tendency towards damage. The continuum model is seen as successfully capturing much of the unique nonlinear trends observed in the molecular dynamics simulations in a volume 1000 times greater than the molecular dynamics unit cell. Additionally, application of the damage model to the continuum unit cell revealed insights into the failure of carbon nanotube reinforced nanocomposites at the sub-microscale.

Introduction

Use of nanoscale fillers such as carbon nanotubes (CNTs) in polymer matrix is gaining importance due to their structural and multifunctional benefits. Understanding the localized effects around CNTs, therefore, in the nanocomposite is necessary for the accurate analysis of their inelastic response. To obtain nanocomposites with the most desirable properties at the structural level, it is important to optimize the nature and volume of the filler material such that only the coveted features are improved while unwanted effects are minimized. To achieve such levels of precision, it is imperative to be able to model and predict the behavior and the effects of CNTs within the polymeric matrix for realistic scenarios. Several techniques that have been used to model polymeric systems with nanoparticles include homogenization,[1] Monte Carlo,[2] and continuum modeling.[3] However, these systems come with various disadvantages, such as loss of relevant information at various length scales, high computation times, and difficulties in local refinement. Molecular dynamics (MD) simulations[4] have shown strong potential in modeling nanocomposites due to the comparable sizes of CNTs and polymer chains. However, the high computational costs associated with

MD simulations limit their use beyond the nanoscale and restrict the simulation time to a few hundred nanoseconds.

One approach to this problem has been to utilize multiscale methods that attempt to capture local effects at certain length scales and then transfer the appropriate information to the next relevant length scale. A few of these methods use a series of continuum-based approaches to calculate the effective properties,[5] multifunctionality,[6] and interphase/interface properties.[7] However, due to the difficulty in modeling stochastic systems at the lowest length scales, periodic structures are generally assumed, which is nonphysical but mathematically straightforward to analyze. Hybrid MD/continuum approaches have also been employed in CNT–polymer systems to calculate variation of moduli with crosslinking degree,[8] linear elastic response,[9] interface damage,[10] effect of orientation and agglomeration on moduli,[11] and elastoplastic behavior.[12] In general, MD/continuum-based multiscale methods have shown great potential for modeling nanomaterial enhanced systems since MD simulations can capture local nonlinear behavior and stochasticity at the lowest length scales while continuum methods scale those phenomenon to higher length scales. Hence, it becomes possible to reproduce accurate elastoplastic and damage behavior of statistically significant amount of CNTs randomly dispersed in the matrix.[13]

In-depth damage investigations that involve MD in a hierarchical multiscale framework has been performed by Yang et al.[12] where the elastoplastic behavior of CNT nanocomposites was estimated from MD simulations at the lower scale and an effective matrix model generated using the domain decomposition method at the higher scale. Recently, the approach of continuum damage mechanics (CDM) has been applied and shown to be very promising in modeling damage. This approach has its roots in metal plasticity, but has been developed for many other applications, such as ceramic matrix composites in a multiscale framework[14] and to describe microcrack distributions in the form of a fourth-order damage included fabric tensor.[15] It has also been shown that the internal state variables (ISVs) concept, which can be used to describe the present state of the material, is compatible with CDM frameworks.[16] Thus, with an arrangement involving CDM and ISVs, it seems possible to implement continuum-based assumptions influenced by MD simulations and polymer mechanics in order to express the damage state of CNT-infused nanocomposites.

Motivated by these requirements towards the modeling of CNTs in polymer matrix, this paper proposes a constitutive law for thermoset polymers based on the framework of CDM with the damage evolution equation developed from the results of elastoplastic MD simulations. This procedure allows damage mechanisms to be physically described from the fundamental damage simulations of CNTs in a polymer matrix. The constitutive equations are derived from the thermodynamic framework proposed by Coleman and Gurtin[17] and the classical CDM methodology as described by

Lemaitre.[18] Additionally, hardening equations are based on polymer physics and special consideration for volumetric damage, and stress triaxialities is applied. The constitutive equation is further applied to a representative volume element (RVE) consisting of a bulk polymer and a sizable number (2000) of CNTs. The proposed continuum model is able to capture the unique stress–strain behavior at localized regions around the CNTs reported by MD simulations. Furthermore, it provides unique insights into the damage mechanism of randomly dispersed CNTs in an epoxy matrix.

This paper is organized as follows: The first section describes the molecular model and the MD simulation procedure. The second section describes the constitutive equations and the evolution formulations motivated by the MD simulations. The third section presents the results of comparison of the proposed damage model against classical formulations, such as the Gurson–Tvergaard–Needleman model and the classical Lemaitre model. The fourth section presents the results of the formulated damage model on a general element with varied parameters. Different case studies are conducted and the predictions of the damage model are illustrated. The fifth section details the CNT generation algorithm. Finally, the sixth section presents the results of the damage model applied to a micro-length scale RVE with randomly oriented CNTs. Parallels between MD simulation results and the finite element (FE) results are emphasized.

The molecular dynamics model

The molecular dynamic model is developed using MD simulations to characterize the linear and nonlinear material response of a nanocomposite at the molecular level. The molecular structures of the epoxy resin and the hardener that constitute the polymer used in this study are di-glycidyl ether of bisphenol F (DGEBF) and di-ethylene tri-amine (DETA), respectively. The details of the stochastic crosslinking approach to perform virtual curing of the epoxy are described in Subramanian et al.[8] MD simulations are performed on the crosslinked polymer systems to obtain the tensile, and shear moduli. Triaxial deformation test simulations are conducted to determine the bulk modulus and isotropy is observed due to the mechanical response of the polymer being independent of the axis of deformation in a system with randomly oriented and well-dispersed CNTs. The variation of mechanical properties (Young's modulus, E and bulk modulus, K) with change in crosslinking degree is linear, shown in Figure 1(a) and (b) and described by the following equation

$$E = 1.59\eta + 1.566K = 1.4907\eta + 6.434 \tag{1}$$
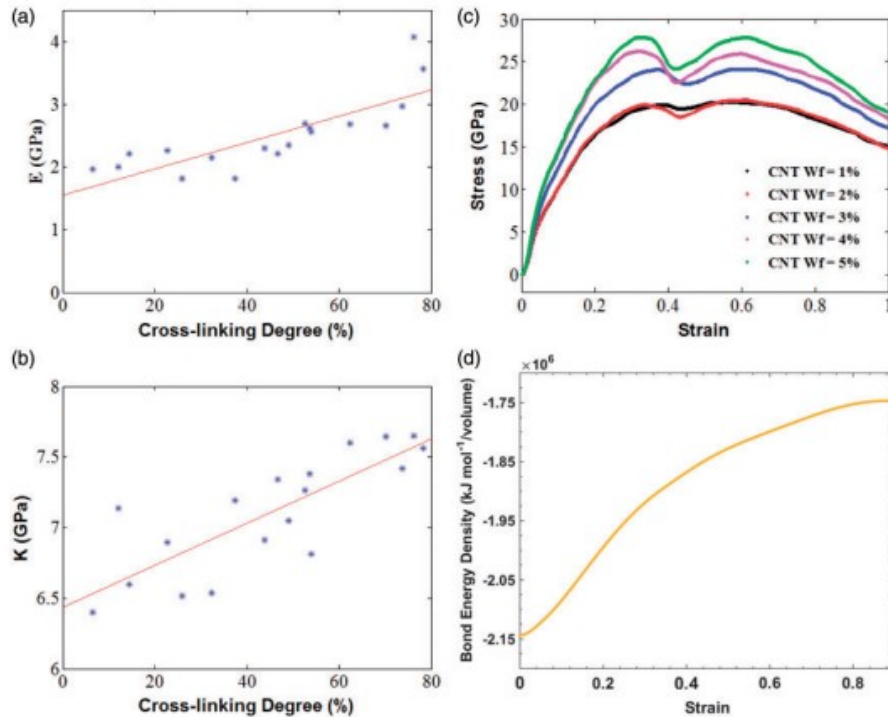
Figure 1. MD model results: (a) variation of elastic modulus with crosslinking degree;[8] (b) variation of bulk modulus with cross-linking degree;[8] (c) stress–strain response for epoxy–CNT system from MD simulations;[8] (d) representative BDE density progression with applied strain.

It is well established that the fundamental cause of plastic behavior in amorphous polymer is the elongation and subsequent breakage of covalent bonds.[19] Traditional MD simulations that use an empirical force field are not capable of capturing bond dissociation between atoms. The external forces propagate through bonds in the matrix and, in turn, the deformation induced by mechanical loading elongates covalent bonds. Thus, in the simulations, a bond order based potential (ReaxFF) is employed to perform deformation tests on a nanoscale representative unit cell (RUC), and to observe the nonlinear response of the CNT epoxy system. The elastoplastic stress–strain response with varying CNT weight fraction in epoxy matrix is illustrated in Figure 1(c). The variation of bond energy between the undeformed, unbound state of the molecular system and at each time step of the deformation test is used to quantify the bond dissociation energy (BDE). The microscale continuum damage model utilizes the BDE quantified for the nanocomposite systems with various CNT weight fractions as input to define the damage parameter. Hence, the variation in bond energy under deformation can be directly related to plastic deformation at the higher length scales. The BDE density curve can be seen in Figure 1(d). Further information on the MD model and the MD stress–strain curve can be found in Subramanian et al.[8,20]

Continuum formulations

The continuum description uses the concept of CDM, the formulations for which have been classically derived by Lemaitre[21] and Chaboche et al.[22] Since, these formulations are based on a thermodynamic framework as defined by Coleman and Gurtin,[23] the free energy has to be specified. The Helmholtz specific free energy is assumed to be a function of the following state variables: the elastic strain $\varepsilon_\sim e$, the isotropic damage variable D and the internal strain like variable associated with chain movement ξ. The hardening variable is explained further in the following sections. The expression for the Helmholtz free energy is

$$\psi = \frac{1}{\rho_0}\bar{\psi}(\varepsilon_\sim e, D, \xi) \tag{2}$$

where ρ_0 is the original density. The total strain can be decomposed into the elastic and plastic strains through an additive decomposition[24] as

$$\varepsilon_\sim = \varepsilon_\sim e + \varepsilon_\sim p \tag{3}$$

Using the Clausius–Duhem inequality, and the assumption of isothermal conditions, the following relation can be obtained

$$\frac{\rho_0}{\rho}\sigma_\sim : \varepsilon_\sim \cdot p + YD\cdot - k\xi\cdot \geq 0 \tag{4}$$

which is the intrinsic dissipation inequality. Y and k are the thermodynamic affinities associated with damage, D and the internal strain due to chain entanglement in the polymer, ξ, respectively. The thermodynamic affinities are defined as

$$Y = -\frac{\partial\bar{\psi}}{\partial D} \qquad \text{and} \qquad k = \frac{\partial\bar{\psi}}{\partial\xi} \tag{5}$$

The free energy term can be additively decomposed to a term that is defined by the elastic energy and a term defined by the hardening variable

$$\bar{\psi} = \bar{\psi}e + \bar{\psi}k \tag{6}$$

The elastic term of the free energy can be obtained using the constitutive relations and the equivalent strain concept[21] as

$$\bar{\psi}e = \frac{1}{2}(1-D)\varepsilon_\sim e : L_\approx : \varepsilon_\sim e \tag{7}$$

where $L_\approx$ is the stiffness matrix. A quadratic hardening free energy term is assumed and can be written as

$$\psi\bar{\ }k = \frac{1}{2}C_k\xi 2 \tag{8}$$

where C_k is the material parameter that represents the internal stresses developed by chain movement and entanglement.

As defined by Chaboche et al.,[22] the density differences can be associated with damage due to volume changes using a dependent variable, D_v

$$\frac{\rho}{\rho_0} = 1 - D_v \tag{9}$$

Using the Coleman arguments and the above relations, the Hooke's law can be obtained as

$$\underset{\sim}{\sigma} = \rho\frac{\partial\psi}{\partial\epsilon^e} = (1-D_v)(1-D)\underset{\approx}{L}:\underset{\sim}{\epsilon}^e \tag{10}$$

The total potential, φ, assumes plastic and damage potentials, φ_p and φ_D. The plastic potential is chosen such that the effects of damage and volumetric change are also considered

$$\varphi = \varphi_p\left(\frac{\rho_0}{\rho}\sigma_\sim, k, D, D_v\right) + \varphi_\xi + \varphi_D \tag{11}$$

The plastic potential, φ_p, considered the yield function is chosen in a similar form as the classical Lemaitre yield function[18]

$$\varphi_p = \frac{\rho_0}{\rho}\frac{\sigma_{cq}^*}{1-D} - k - \sigma_y \leq 0 \tag{12}$$

where σ_y represents the yield stress. The equivalent stress σ_{cq}^* is chosen such that hydrostatic stresses can be considered. Hence, a combination of the first and second invariants is taken using a variable elliptic form as used in works of Green and Besson[25,26] and Chaboche et al.[22]

$$\sigma_{cq}^* = J(\sigma_\sim)2 + \alpha f(D, D_v)I(\sigma_\sim)2 \tag{13}$$

where α is the degree of ellipticity and is taken to be 0.5 in this work. (D, D_v) is a function of the damage parameters used to couple the yield function with the associated damage. In this paper, this function is assumed to be varying only with volumetric damage and specified as $f(D, D_v) = D_0 + D_v$ where D_0 is a small phenomenological constant used to couple hydrostatic stresses with the deviatoric components even when D_v is 0. When α is 0, the yield function reduces to the classical Lemaitre form.

Evolution of state variables

Plastic strain: Using the normality considerations we can denote the plastic strain rate as

$$\varepsilon_{\sim} \cdot p = \lambda \cdot \frac{\partial \varphi}{\partial(\frac{p_0}{\rho} \sigma_{\sim})} = \frac{\lambda \cdot}{1 - D} \frac{\partial \sigma_{eq}^*}{\partial \sigma_{\sim}} \tag{14}$$

where the viscoplastic multiplier is obtained using the Peric formulations as described in the study by Perić,[27] and is shown below

$$\lambda \cdot = \frac{1}{K} \left[\left(\frac{\varphi + \sigma_y}{\sigma_y} \right) \frac{1}{n} - 1 \right] \tag{15}$$

where K and n are the viscoplastic constants.

Internal strain: In general, it is understood that the physics of polymer hardening are vastly different from that of metals due to the nature of polymeric materials; as such, the physics of polymer chain motion and entanglement is simulated with an internal strain like quantity. The evolution of the internal strain due to chain entanglement ξ is described by evolution equations formulated by Anand and Gurtin.[28] The equation as simplified by Bouvard et al.[29] is described as follows

$$\xi \cdot = h_0 \left(1 - \frac{\xi}{\xi^*} \right) \lambda \cdot \qquad \xi \cdot ^* = g_0 \left(1 - \frac{\xi^*}{\xi_{sat}} \right) \lambda \cdot \tag{16}$$

The evolution equation for the internal strains describes obstacles to chain movements such as chain entanglement points. The internal strain produced due to these obstacles and the resultant entanglement can be described by ξ. The energy barrier that opposes chain movement is described by the term ⬚*. As more chains escape the entanglement points, there is a lowering of the energetic barrier, which results from an increase of cooperative motion of chains. Hence, ⬚* decreases as ξ increases until the saturation point ξ_{sat} is reached. h_0 and g_0 are the associated hardening moduli. The internal stresses due to chain entanglement in the polymer network are described by

$$k = \frac{\partial \psi^-}{\partial \xi} = C_k \xi \tag{17}$$

Damage: For thermoset polymers under isothermal conditions and at operating temperatures below the glass transition temperature, the energy variations due to successive bond breakages at the atomistic scale has been shown to be related to damage at the continuum level.[20] Therefore, a new

damage evolution law at the continuum scale is formulated based on the fundamental damage occurring in the polymer. A sigmoidal damage evolution law, with parameters varying according to crosslinking degree, is used following the BDE trend observed in MD simulations. It is observed physically and through MD simulations that the polymer stiffness is a function of the crosslinking degree.[8] Also, at low crosslinking degree, i.e. low curing, the polymer exists in a viscous state where damaging the material requires application of minimal energy. At high crosslinking degree, i.e. high curing, the polymer is stiff requiring higher application of energy to damage. Hence, the damage evolution is chosen so that it reflects the change of the nature of damage with change in crosslinking degree. Thus it is expressed as

$$D_\cdot = \frac{\lambda_\cdot}{2} \cdot \left[\mathrm{sgn}(\chi) \cdot \frac{-(1-\eta)|\chi| - |\chi|}{-2(1-\eta)|\chi| + (1-\eta) - 1} + 1 \right] \tag{18}$$

where sgn() is the signum function and χ is defined as

$$\chi = 2\left(\frac{Y}{Y_0}\right)^{\frac{1}{2(1-\eta)}} - 1 \tag{19}$$

η is the crosslinking degree and Y_0 is a material parameter associated with the maximum energy required to begin damaging the material. Figure 2 shows the variation of nominal rate of damage $\dot{D}_\cdot (\lambda_\cdot = 1)$ versus normalized elastic energy $\frac{Y}{Y_0}$.
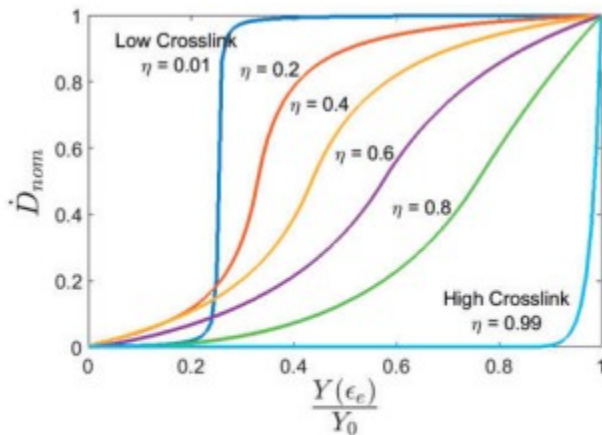
Figure 2. Damage evolution for a spectrum of crosslinking degrees.

Volumetric damage: The volumetric damage evolution is simply obtained through the equations of mass conservation of volume changes induced due to plasticity. It can be written as

$$\dot{D}_v = (1 - D_v)Tr\left(\dot{\underline{\epsilon}}^p\right) \tag{20}$$

Yield stress variation with crosslinking

Since, the analysis in this paper considers variation of material behavior with the polymer crosslinking degree, a relationship between yield stress σ_y and crosslinking degree η needs to be determined. In this work, this relationship is found through experimental procedures. The experimental procedure detailed by Fard et al.[30] was followed. A uniaxial quasi static test of a flat dog-bone specimen made from Epon E863 Resin and Epi-Cure 3290 hardener (100/27 weight ratio) was performed. To find the relationship between crosslinking degree and yield stress, specimens were tested for different total cure times. The curing times for the tested specimens are shown in Table 1. Since specimens are cured for different amounts of time, the hypothesis is that each specimen will have a different crosslinking degree, since crosslinking degree is a function of the curing time and temperature. The temperature of the room where the specimens were cured was kept constant and similar for all specimens throughout the curing process; hence the temperature is not considered to be a curing variable.

Table 1. Specimen cure times.

Specimen Number	Curing time (h)
Specimen 1	6.5
Specimen 2	7
Specimen 3	7.5
Specimen 4	8

From the test results, the elastic modulus of each specimen was calculated using standard procedures for uniaxial tests. The yield stress for each specimen was calculated as the first point of nonlinearity of the stress–strain curve.

Using equation (1), the crosslinking degree for each specimen was back calculated. The relationship between crosslinking degree and the corresponding yield stress was then plotted and can be seen in Figure 3. The linear model fit was found to have the equation

$$\sigma_y = 37.495\eta + 56.249$$
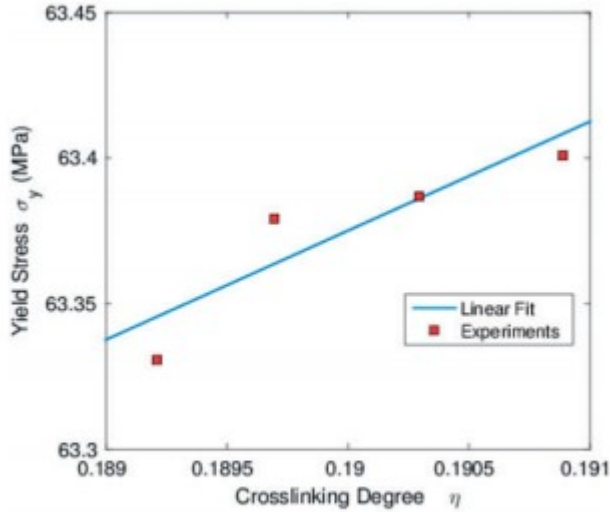
Figure 3. Yield stress vs crosslinking degree.

CDM formulation benchmarking

The proposed damage model is benchmarked against two widely used classical porous plasticity models present in the literature, the Gurson model as modified by Tvergaard and Needleman[31] and the classical Lemaitre CDM model.[18,21] Realistic material parameters for an aerospace grade polymer are provided to the Gurson–Tvergaard–Needleman(GTN) model. Subsequently, the Lemaitre CDM model is fitted to match the GTN model by changing the values of parameters associated with Lemaitre's damage evolution law. Following this, the proposed model is provided with the same parameters as applied to the Lemaitre CDM model. To ensure a similar basis for comparison, all three models are provided with the same hardening definition as explained in the "Continuum formulation" section and additional parameters detailed in Table 3. The model specific parameters are detailed in Table 2. The reader is referred to the documentation of Abaqus 6.13, which details the formulations of the GTN model and explanation of the parameters.[32] The classical Lemaitre damage evolution equation used in this section is expressed as:

$$D\cdot = (\tfrac{Y}{S})s(1 - D) - \beta + 1\lambda\cdot .$$

Table 2. Model parameters.

	GTN		Lemaitre
η	0.19	η	0.19
σ_y	63.75 MPa	σ_y	63.75 MPa
q1	1.5	S	1×10^7 J/m3
q2	1	s	1
q3	1	Y	.12 MPa
f_c	0.1	β	1
f_F	0.4		
f_N	0.08		
μ_N	0.05		
s_N	0.01		

Table 3. Damage model parameters.

| η	.19	h_0	2
$\dot{\epsilon}$	.005 per second	g_0	1
K	15	ξ_{sat}	0.08
n	2.5	ξ_0	0.12
σ_y	63.375 MPa	C_k	2.8 GPa
Y_0	.12 MPa		

The comparison of the three models can be seen in Figure 4. It is observed that the GTN model underestimates initial damage until the critical porosity volume fraction is reached. The critical porosity volume fraction can be a subjective parameter and is hard to define especially for polymers. The classical CDM model overestimates damage due to the exponential damage evolution function it uses. The model developed in the "Continuum formulations" section shows the same trend as the classical models until substantial nonlinearity is observed followed by stable damage evolution. This trend seems to correlate with physical evidence that damage evolution is slow initially, followed by a faster rate as cracks coalesce and subsequently followed by a slower rate as the damaged state saturates.
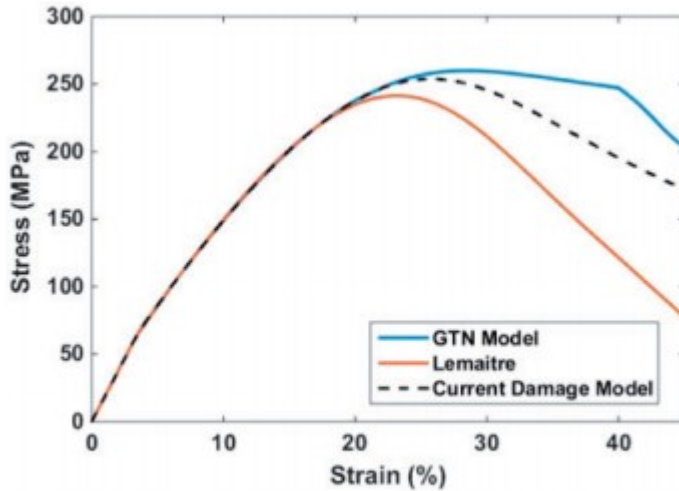
**Figure 4.** Model benchmarking.

Damage model results

This section presents results and predictions from the proposed damage model. Figure 5(a) shows the comparison of the damage model to a uniaxial tension experiment.[30] From the experimental values, it is possible to calculate the crosslinking degree by performing an inverse calculation for the modulus using equation (1). The crosslinking degree was calculated to be ⬚=.19, in the performed experiments. This value was used as input to the damage model, and the rupture criteria D_c defined as the percentage of damage at which global material failure occurs, was set to be 2.5%. Figure 5(c) shows the predictions of the model with D_c set to 30%. The parameters used are detailed in Table 3. The simulation showed good correlation with experimental results using these parameters. Further computations were performed using these parameters; results of these simulations are shown in the subsequent sections:
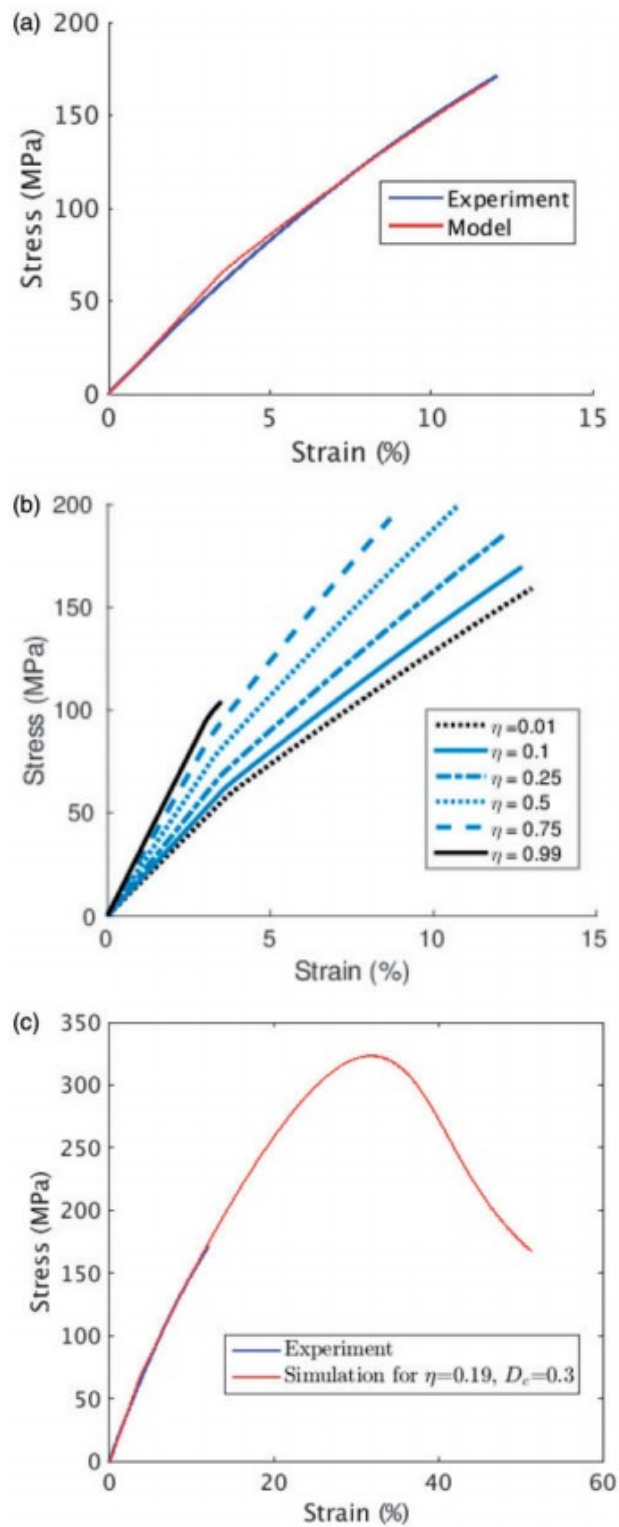
Figure 5. Stress–strain curves predicted by proposed model: (a) model and experiment comparison with $D_c = 2.5\%$; (b) simulated stress—strain response for varying crosslinking degree; (c) stress–strain response with $D_c = 30\%$.

Variation with crosslinking degree: The variation of stress–strain response with crosslinking degree is shown in Figure 5(b). At low crosslinking degrees, the model predicts greater post yield behavior while at higher crosslinking degrees, the post yield region decreases considerably. The maximum ultimate strength is reached at about 60% crosslinking, subsequent to which, there is a quick lowering of ultimate strength. At high crosslinking degrees, the model predicts a behavior wherein the material fails with almost no post yield response, which is similar to a brittle material response.

Internal state variable evolution: The evolution of the damage variable D and the damage evolution $\dot{D}$ is shown in Figure 6(a) for two extreme values of the crosslinking degree at $\dot{\epsilon}=2.5\%$. It is observed that at lower crosslinking degree, the damage evolution is slower, whereas at higher crosslinking degree, damage evolution is more rapid. This trend implies that at lower crosslinking degree, a larger post yield response can be expected while smaller post yield region can be expected for higher crosslinking degree. Figure 6(b) shows the damage variables D and $\dot{D}$ for crosslinking degree $\chi=.19$ and $\dot{\epsilon}=30\%$. The effects of the sigmoidal damage evolution on the damage variable can be seen in these figures. The initial increase in damage evolution is caused by initiation of damage and is followed by a nonlinearly increasing damage profile, which can be attributed to progressive damage. This state leads to a peak in damage evolution causing a saturated state of damage in the material. Following the peak, there is a decrease in the rate of damage, which consequently decreases damage accumulation.
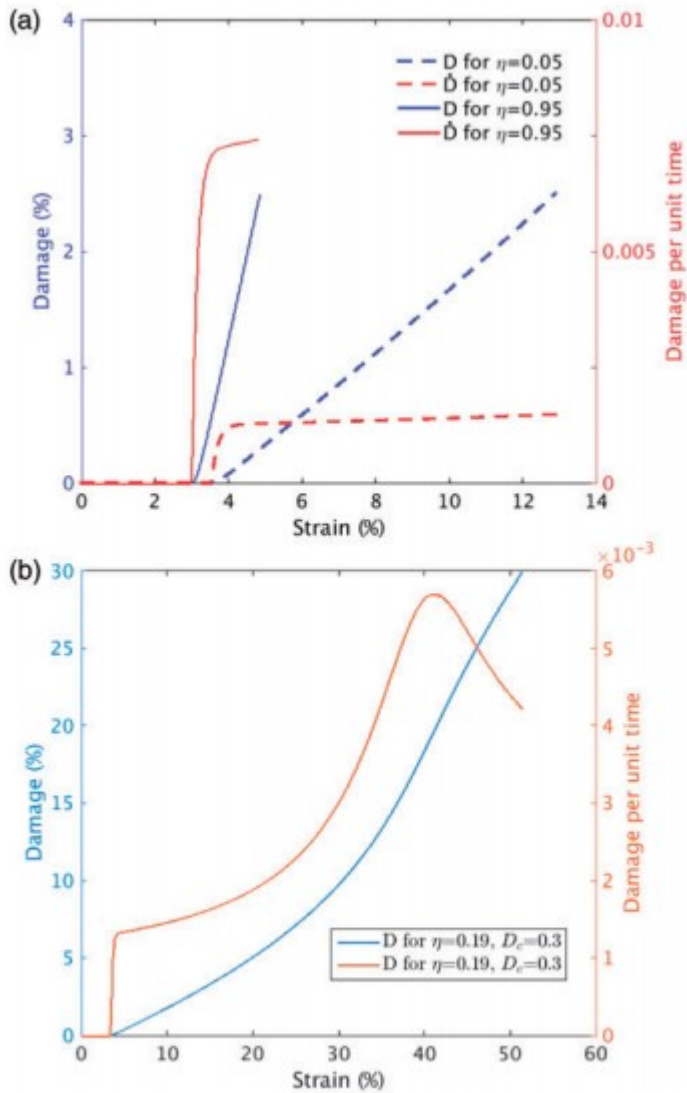
Figure 6. Simulation of damage parameters: (a) at $\eta = 0.05$ and $\eta = 0.95$ with $D_c = 2.5\%$; (b) at $\eta = 0.19$ with $D_c = 30\%$.

Hardening parameter evolution: The evolution of the hardening parameters is shown in Figure 7(a). It can be seen that ▯* decreases as ξ increases until eventually the saturation values are reached. ξ displays the internal strain due to chain entanglements and obstacles to chain movement. As chain movement increases and the associated energy increases; the barrier to this movement, displayed by ▯* decreases, leading to more chain movement and continued decrease of chain entanglement. At lower strains this phenomenon is a major cause of hardening and softening in polymers.[28,29] Figure 7(b) shows the hardening parameter evolution for ▯=.19 and ▯▯=30%. This figure clearly illustrates the state at which saturation has been attained and, hence, there is an equalization of ξ and ▯*.
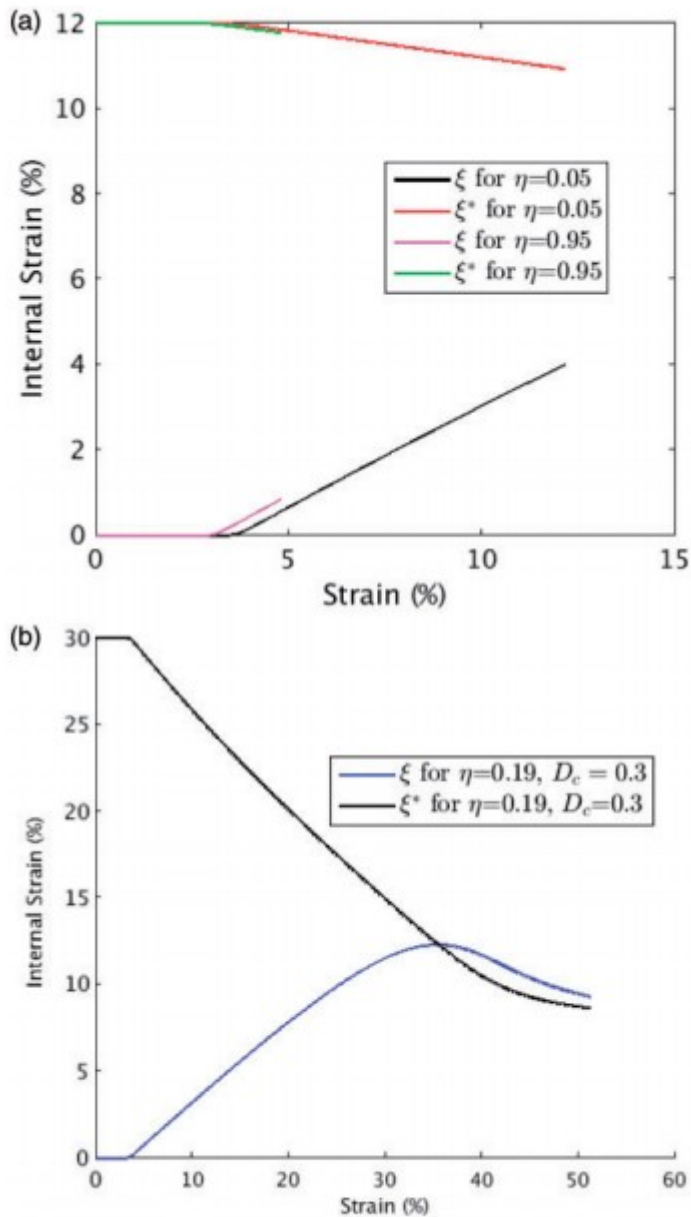
Figure 7. Simulation of hardening parameters: (a) at $\eta = 0.05$ and $\eta = 0.95$ with $D_c = 2.5\%$; (b) at $\eta = 0.19$ with $D_c = 30\%$.

## Generation of the micro-length scale model

The damage model developed in the previous sections is incorporated into a microscale model to investigate effects of dispersed CNTs in polymer. Hence, microscale RVEs of the polymer with CNTs are explicitly modeled. The CNTs are modeled separately, and incorporated into the polymer model. This section details the CNT generation algorithm. The CNTs are randomly generated with the vertices of the CNTs calculated using the transformation formula

$$x = L_{CNT}1 - \varphi 2 \cos(\theta)y = L_{CNT}1 - \varphi 2 \sin(\theta)z = L_{CNT}\varphi \qquad (21)$$

where x, y, z are the coordinates of the vertices of the CNT in the global coordinate system of the FE model, $\theta = 2\pi\alpha$, $\varphi = 2\alpha - 1$ and α is randomly generated with a value between 0 and 1. L_{CNT} is the length of a segment of the CNT generated. Figure 8 shows a schematic of the CNT generation algorithm. The schematic contains three segments and four vertices for illustrative purposes; however, the generated CNT geometries contain seven segments with eight vertices per CNT, along with 3D waviness. Using equation (21), coordinates of each vertex of the CNT geometry, x_i,y_i,z_i, in the global FE coordinate system is obtained. This procedure is used to calculate the vertices for 2000 CNTs leading to a total of 16,000 vertex points per FE model of the micro-RVE. The randomized transformation formula imparts waviness to the CNTs, thus creating realistic CNT geometries rather than perfectly straight idealized CNT geometries. The number of CNTs in a model remains constant at 2000. The unit cell dimensions are varied in order to alter the weight fraction of the CNTs in the micro-RVE. The material properties and dimensions of the CNTs are obtained from Romanov et al.[33] and are reported in Table 4. The randomly generated CNTs are shown in Figure 9. Three dimensional truss elements were used to model the CNTs with eight nodes per CNT since the CNTs provide structural reinforcement in the matrix and also since investigating the stress variation through the CNTs is not of interest in this study. Furthermore, periodic boundary conditions are utilized to simulate periodicity of the RVE.[36-38] Figure 13 shows the difference in response of the model with and without periodic boundary conditions.
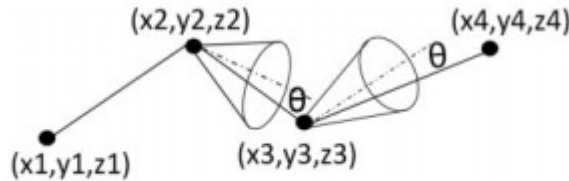
Figure 8. Schematic of the CNT generation algorithm.

Table 4. Table of CNT properties.

|	
CNT length	0.5 µm
CNT diameter	9 nm
Type	Single walled
Elastic modulus	475 GPa
N	0.35
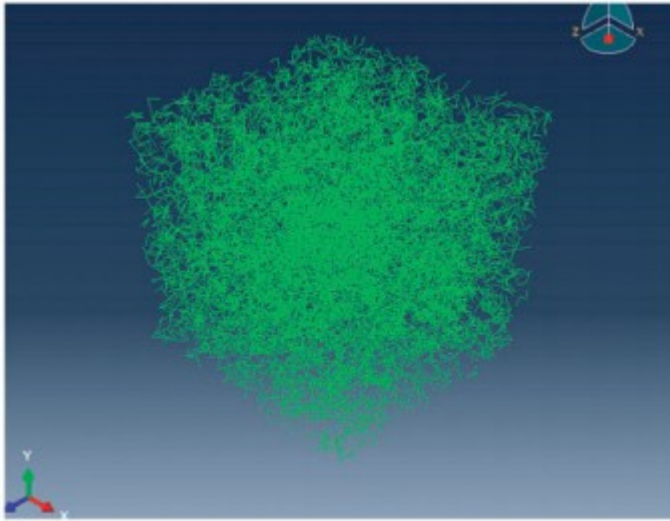
Figure 9. Randomly oriented CNT mesh.

Using conventional meshing techniques, the polymer elements would have to be meshed along with the CNT elements, which would call for fine local meshing and a complicated mesh structure at the interface between the CNTs and the polymer. Hence, the technique of embedded elements is used to achieve the meshing required in this case.[33,34] Embedded meshes are used to embed a large group of target elements inside a region of host elements, through which the translational degrees of freedom of the target elements are constrained according to the response of the host elements. The polymer matrix host mesh uses 5000 elements of fully integrable 8-noded 3D solid C3D8 brick elements.

Microscale model results

Micro-length scale RVEs of polymer matrix with periodic boundary conditions and embedded CNTs were generated using the CNT generation algorithm. The CNTs were modeled and inserted into a bulk polymer model using the embedded mesh technique.[33] The results of the micromechanical model with an RVE containing the polymer matrix and randomly generated CNTs are presented here. The model is simulated in the commercial Finite Element Package Abaqus 6.13 with the damage equations implemented in a user material subroutine. The simulations are conducted using unidirectional loading under a constant strain rate of 0.005 strain per second.

Local damage: Figure 10 shows the comparison of damage contours between a model that contains neat epoxy and a model containing CNTs in an epoxy polymer. It can be seen that the presence of CNTs causes local damage.
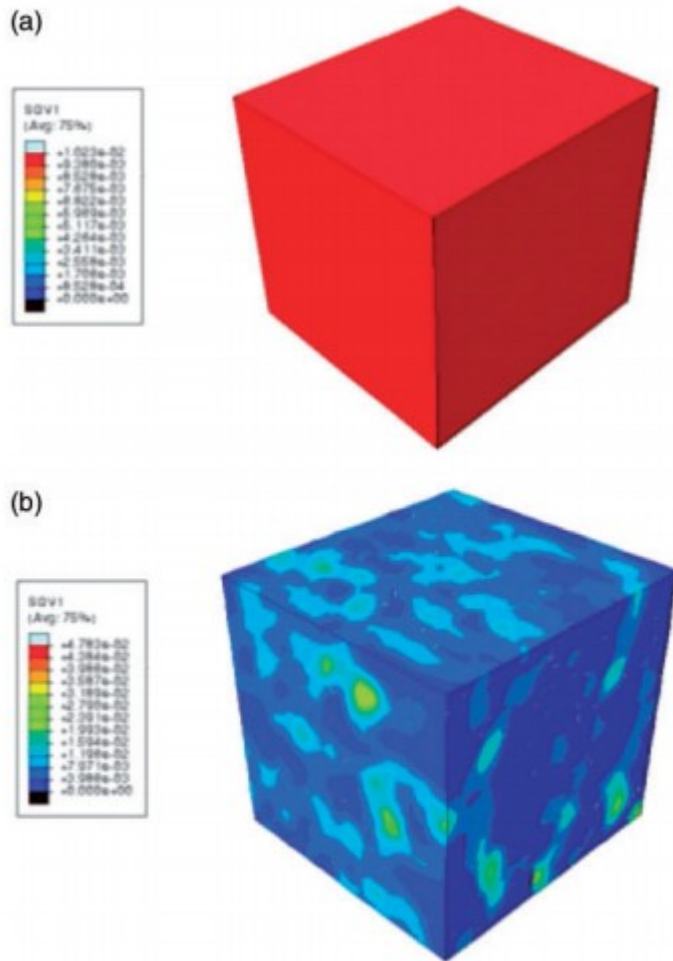
Figure 10. (a) Isotropic damage contour with no CNTs; (b) local damage contours due to presence of CNTs.

Comparison of MD and FE response: Figure 11 shows the global stress–strain response of a 1% weight fraction CNT–polymer RVE compared to the stress–strain response of a local region around a single CNT. As seen from Figure 11, the local stress–strain response in the vicinity of the CNTs exhibits an initial drop in stress followed by a recovery phase. The local response around the CNTs displays a similar trend as seen in MD simulations of the CNT-polymer RVE as shown in Figure 1(c). However, it is observed that the global response of the RVE does not show the recovery phenomenon observed in the MD results. The elastoplastic response predicted by the continuum model in the vicinity of the CNT and the response from the MD model exhibit a highly localized behavior, while the global response displays a more spatially averaged response. This implies that there is high spatial variation in the stress–strain response within the RVE and that although the average response demonstrates isotropic behavior, locally the RVE is not isotropic.
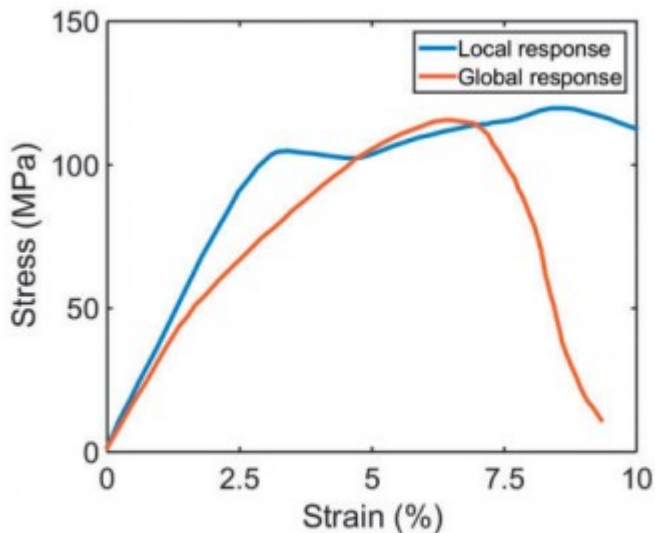
Figure 11. Global stress–strain response of the RVE compared with stress–strain response of local regions around the CNT.

Local damage evolution: The characteristic stress–strain trend at local CNT-rich regions, labeled "local response" in Figure 11, can be explained from parallel discrete and continuum viewpoints. From a nanoscale perspective, the initial elastic region of the stress–strain curve indicates the stretching of bonds in the CNTs and the polymer chains due to mechanical deformation. The yield point followed by softening, which leads to the first dip in the stress–strain curve as seen in Figure 1(c) corresponds to bond scission of the weaker covalent bonds. Subsequently, the polymer chains become taut and molecular chain sliding initiates, resulting in the hardening observed in the stress–strain curve, referred to as the recovery phase in the previous subsection. The final stress drop indicates successive bond dissociation in the molecular system resulting in failure. From the continuum perspective, the stress–strain response can be explained by the local damage evolution trend shown in Figure 12. The damage curve shows a peak that corresponds to the first drop in stress seen in the local stress–strain curve of Figure 11. After the initial peak, the damage rate decreases and then evolves at a controlled rate. This explains the drop in stress at higher strains past the recovery phase seen in the local stress–strain curve. The high stiffness provided by the CNTs allow a large amount of the load to be carried locally by the CNTs until a point is reached where there is a separation between the CNT group and the polymer around it. This corresponds to the first peak in the damage evolution curve in Figure 12 and the corresponding dip in the local stress–strain curve seen in Figure 11. After the separation occurs, a more meaningful and natural load division occurs between the CNTs and the polymer, and further damage occurs as a normal progression of cracks in the flawed material. This effect can be observed after the peak in the damage evolution curve.
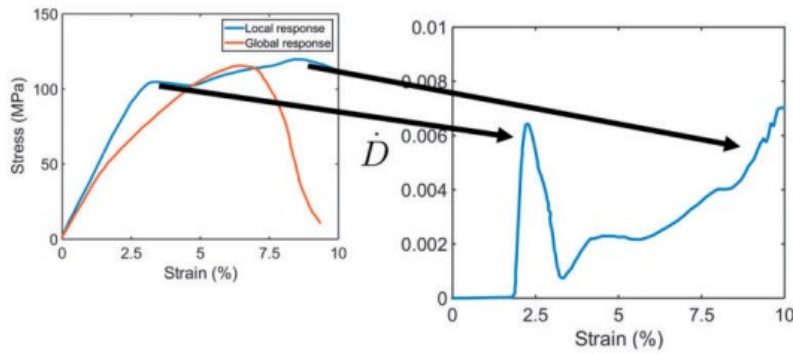
Figure 12. Damage evolution in the continuum model at local regions around the CNT compared with local stress–strain response.
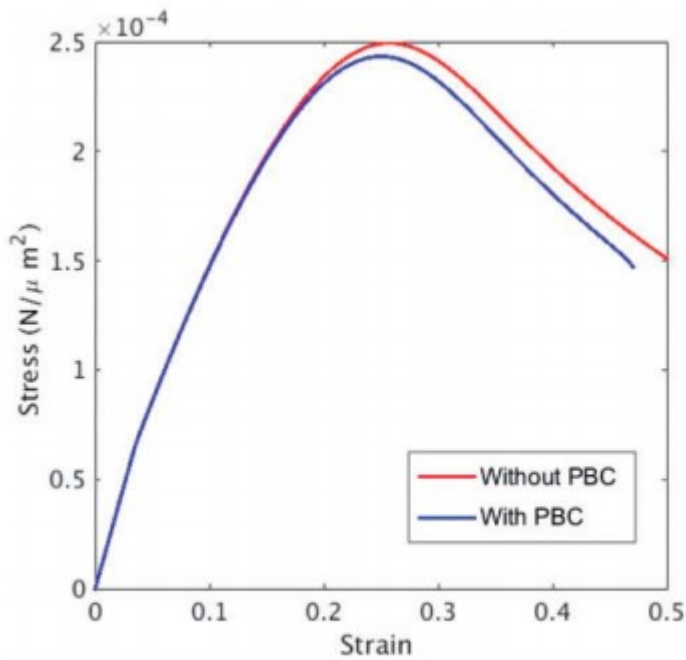
Figure 13. Result of the damage model after applying periodic boundary conditions (PBCs).

Conclusion

In this paper, a CDM-based formulation was developed to quantify the damage in polymers. A novel damage evolution methodology, based on bond breakage simulations from MD simulations, was developed. This formulation was used in a micromechanical model with the RVE containing polymer and CNTs in a randomly dispersed configurations. Through these simulations insights on how CNTs behave within a polymeric volume were gained as follows:

1. Damage evolution due to bond breakage is observed to follow a sigmoidal trend, which can be utilized in CDM-like formulations. The

behavior of the polymer can then be related to its crosslinking degree, which can be used to characterize stiffness and damage parameters.

2. The results from micromechanics, especially local response trends, match very well with MD results, indicating the validity of the BDE approach and the effectiveness of bridging between length scales.

3. The unique stress–strain response obtained from CNT–epoxy MD simulations is also observed in an RVE of larger scale that contains a statistically significant number of CNTs; however, this is found to be a highly localized phenomenon occurring immediately next to the CNTs. Moreover, this takes place as a result of the local load transfer caused by CNT stiffness, and the subsequent separation of the polymer from the CNT surface.

4. The characteristic initial decrease in stress and the subsequent recovery observed in the local stress–strain response curve seems to be caused by a similar phenomenon, both in the MD simulations and the continuum simulations. This phenomenon is produced due to the nature of localized damage and the concentration difference between CNT and the surrounding polymer matrix.

With the development of this methodology and insights provided in this paper, it is clear that better multiscale models of CNT–polymers can be built that accurately predict damage and explain the highly complex damage phenomenon in nanocomposites. This also highlights the need for atomistic as well as continuum methods for the analysis of nanostructure deformation. Many hierarchical methods in multiscale methodologies construct a macro-level material tensor by solving boundary value problems at the micro-length scale RUCs.[35] Such methodologies can benefit from the model presented in this paper by the inclusion of nonlinear effects leading to top-down and bottom-up predictive multiscale capabilities and optimization of nanostructure architecture.[36-38]

References

1.

Seidel, GD, Lagoudas, DC. Micromechanical analysis of the effective elastic properties of carbon nanotube reinforced composites. Mech Mater 2006; 38: 884–907.

2.

Valavala, P, Odegard, G. Modeling techniques for determination of mechanical properties of polymer nanocomposites. Rev Adv Mater Sci 2005; 9: 34–44.

3.

Fish, J, Wagiman, A. Multiscale finite element method for a locally nonperiodic heterogeneous medium. Comput Mech 1993; 12: 164–180.

4.

Rahmat, M, Hubert, P. Carbon nanotube–polymer interactions in nanocomposites: A review. Compos Sci Technol 2011; 72: 72–84.

5.

Spanos, P, Kontsos, A. A multiscale Monte Carlo finite element method for determining mechanical properties of polymer nanocomposites. Probab Eng Mech 2008; 23: 456–470.

6.

Ren, X, Burton, J, Seidel, GD. Computational multiscale modeling and characterization of piezoresistivity in fuzzy fiber reinforced polymer composites. Int J Solids Struct 2015; 54: 121–134.

7.

Spanos, K, Georgantzinos, S, Anifantis, N. Investigation of stress transfer in carbon nanotube reinforced composites using a multi-scale finite element approach. Compos Part B: Eng 2014; 63: 85–93.

8.

Subramanian, N, Rai, A, Chattopadhyay, A. Atomistically informed stochastic multiscale model to predict the behavior of carbon nanotube-enhanced nanocomposites. Carbon 2015; 94: 661–672.

9.

Zhang, J, Koo, B, Subramanian, N. An optimized cross-linked network model to simulate the linear elastic material response of a smart polymer. J Intell Mater Syst Struct 2015.

10.

Namilae, S, Chandra, N. Multiscale model to study the effect of interfaces in carbon nanotube-based composites. J Eng Mater Technol 2005; 127: 222–232.

11.

Alian, A, Kundalwal, S, Meguid, S. Multiscale modeling of carbon nanotube epoxy composites. Polymer 2015; 70: 149–160.

12.

Yang, S, Yu, S, Ryu, J. Nonlinear multiscale modeling approach to characterize elastoplastic behavior of CNT/polymer nanocomposites considering the interphase and interfacial imperfection. Int J Plast 2013; 41: 124–146.

13.

Yang, S, Cho, M. Scale bridging method to characterize mechanical properties of nanoparticle/polymer nanocomposites. Appl Phys Lett 2008; 93.

14.

Shojaei, A, Li, G, Fish, J. Multi-scale constitutive modeling of ceramic matrix composites by continuum damage mechanics. Int J Solids Struct 2014; 51: 4068–4081.

15.

Voyiadjis, GZ, Kattan, PI. Damage mechanics with fabric tensors. Mech Adv Mater Struct 2006; 13: 285–301.

16.

Horstemeyer, MF, Revelli, V. Stress history dependent localization and failure using continuum damage mechanics concepts. ASTM Special Tech Publ 1997; 1315: 216–237.

17.

Coleman, BD, Gurtin, ME. Thermodynamics with internal state variables. J Chem Phys 1967; 47: 597–613.

18.

Lemaitre, J . A continuous damage mechanics model for ductile fracture. J Eng Mater Technol 1985; 107: 83–89.

19.

Grellmann, W, Seidler, S. Deformation and fracture behaviour of polymers, New York: Springer Science & Business Media, 2013.

20.

Subramanian N, Koo B, Rai A, et al. A multiscale damage initiation model for CNT-enhanced epoxy polymers. In: *20th international conference on composite materials*, Copenhagen, Denmark, 19–24 July 2015, pp. 4410–4418.

21.

Lemaitre, J . A course on damage mechanics, New York: Springer Science & Business Media, 2012.

22.

Chaboche, J, Boudifa, M, Saanouni, K. A CDM approach of ductile damage with plastic compressibility. Int J Fract 2006; 137: 51–75.

23.

Coleman, JN, Khan, U, Blau, WJ. Small but strong: A review of the mechanical properties of carbon nanotube– polymer composites. Carbon 2006; 44: 1624–1652.

24.

Jeridi, M, Laiarinandrasana, L, Sai, K. Comparative study of continuum damage mechanics and mechanics of porous media based on multi-mechanism model on polyamide 6 semi-crystalline polymer. Int J Solids Struct 2015; 53: 12–27.

25.

Green, R . A plasticity theory for porous solids. Int J Mech Sci 1972; 14: 215–224.

26.

Besson, J, Guillemer-Neel, C. An extension of the Green and Gurson models to kinematic hardening. Mech Mater 2003; 35: 1–18.

27.

Perić, D . On a class of constitutive equations in viscoplasticity: Formulation and computational issues. Int J Numer Meth Eng 1993; 36: 1365–1393.

28.

Anand, L, Gurtin, ME. A theory of amorphous solids undergoing large deformations, with application to polymeric glasses. Int J Solids Struct 2003; 40: 1465–1487.

29.

Bouvard, J, Ward, D, Hossain, D. A general inelastic internal state variable model for amorphous glassy polymers. Acta Mech 2010; 213: 71–96.

30.

Fard, MY, Liu, Y, Chattopadhyay, A. Characterization of epoxy resin including strain rate effects using digital image correlation system. J Aerosp Eng 2011; 25: 308–319.

31.

Tvergaard, V, Needleman, A. Analysis of the cup-cone fracture in a round tensile bar. Acta Metall 1984; 32: 157–169.

32.

ABAQUS/Standard analysis user's manual version 6.13-2, Providence, RI: Dassault Systémes Simulia Corp., 2013.

33.

Romanov, VS, Lomov, SV, Verpoest, I. Modelling evidence of stress concentration mitigation at the micro-scale in polymer composites by the addition of carbon nanotubes. Carbon 2015; 82: 184–194.

34.

Dolbow, J, Harari, I. An efficient finite element method for embedded interface problems. Int J Numer Meth Eng 2009; 78: 229–252.

35.

Barbero, EJ . Finite element analysis of composite materials using Abaqus^{Tm}, Boca Raton, FL: CRC Press, 2013.

36.

Pellegrino, C, Galvanetto, U, Schrefler, B. Numerical homogenization of periodic composite materials with non-linear material components. Int J Numer Meth Eng 1999; 46: 1609–1637.

37.

Segurado, J, Llorca, J. A numerical approximation to the elastic properties of sphere-reinforced composites. J Mech Phys Solids 2002; 50: 2107–2121.

38.

Chen, Y, Ghosh, S. Micromechanical analysis of strain rate-dependent deformation and failure in composite microstructures under dynamic loading conditions. Int J Plast 2012; 32: 218–247.